Anomalous two-photon spectral features in warm rubidium vapor

C. Perrella,[1] P. S. Light,[1] T. J. Milburn,[2,3,*] D. Kielpinski,[4,5] T. M. Stace,[2] and A. N. Luiten[1]

[1]*Institute for Photonics and Advanced Sensing (IPAS) and the School of Physical Sciences, The University of Adelaide, Adelaide, Australia*
[2]*ARC Centre for Engineered Quantum System, Department of Physics, University of Queensland, Brisbane QLD 4072, Australia*
[3]*Institute of Atomic and Subatomic Physics, Vienna University of Technology, Stadionallee 2, 1020 Vienna, Austria*
[4]*Centre for Quantum Dynamics and Australian Attosecond Science Facility, Griffith University, Nathan QLD 4111, Australia*
[5]*Centre of Excellence for Coherent X-Ray Science, Griffith University, Nathan QLD 4111, Australia*

We report observation of anomalous fluorescence spectral features in the environs of a two-photon transition in a rubidium vapor when excited with two different wavelength lasers that are both counterpropagating through the vapor. These features are characterized by an unusual trade-off between the detunings of the driving fields. Three different hypothetical processes are presented to explain the observed spectra: a simultaneous three-atom and four-photon collision, a four-photon excitation involving a light field produced via amplified spontaneous emission, and population pumping perturbing the expected steady-state spectra. Numerical modeling of each hypothetical process is presented, supporting the population pumping process as the most plausible mechanism.

I. INTRODUCTION

The understanding of complex interactions between light and atoms to produce particular optical absorption characteristics has been an active area of research for many years [1]. For example, complex light-atom interaction has been induced in three-level atomic media using electromagnetically induced transparency [2,3], electromagnetically induced absorption [3,4], coherent trapping of atomic populations [5], and quantum interference between atomic energy levels [6]. These coherent processes have been the basis for highly sensitive magnetometers [7,8], quantum information processing using Kerr-type nonlinearities [9], efficient photon-counting [10,11], frequency up-conversion using atomic vapors [12,13], lasing without population inversion [6], and highly compact frequency standards [14,15].

The possibility for multiphoton interactions [16] offers a platform for many other applications because they provide a means for modulation, or sensing, of one light field with another. These transitions have found applications in all-optical switches [11,17,18], single-photon generation [19], and photon coherence measurements and quantum logic gates [20,21]. Furthermore, multiphoton transitions can excite into long-lived atomic states with their inherently narrow linewidths: these have been beneficial for frequency metrology applications such as atomic clocks and frequency stabilization [22,23].

It is also possible for atom-atom interactions, mediated via long-range dipole-dipole coupling, to produce observable effects in the optical absorption of atomic vapors [24–26]. Typically observed in ultracold atomic clouds [27–29], long-range dipole-dipole interactions have been recently observed in thermal rubidium and potassium vapors [24,26]. Such interactions have also been proposed for applications as broad as quantum information processing schemes [30] to atomic clocks [30] as well as for creation of novel quantum states of matter [31] and Rydberg-state quantum gates and molecules [28].

In this paper we report observations of a number of anomalous spectral features in the two-photon transition fluorescence spectra observed in a room-temperature rubidium (Rb) vapor

when excited with two different wavelength lasers that were both counterpropagating through the vapor. We present three hypothetical mechanisms that satisfy the observed energy relationships: (i) triatomic bound states in which a triatomic molecule resonantly absorbs four photons, (ii) amplified spontaneous emission of an auxillary field to produce a four-photon resonance, and (iii) optical pumping that depletes the active atomic ground state to produce an anomalous feature. We model each of these situations numerically and conclude that, although all three mechanisms produce resonant features in common with experimental observations, only the third explanation is consistent with all the experimental results.

II. EXPERIMENTAL SETUP

The anomalous spectral features were observed using the $5S_{1/2} \rightarrow 5D_{5/2}$ two-photon transition of both ^{85}Rb and ^{87}Rb [32]. Driving lasers and relevant decay routes of the atomic transitions are depicted in Fig. 1(a). The $5D_{5/2}$ excited state has a lifetime of 238 ns (linewidth of 666 kHz) [33]. The two-photon transition strength is enhanced by driving it with two different color lasers at 780 and 776 nm, which delivers a near-resonant intermediate state: the intermediate state, $5P_{3/2}$, has a lifetime of 26.2 ns (linewidth of 6.1 MHz) [34]. Excitation into the $5D_{5/2}$ excited state was monitored using the 420-nm fluorescence produced when the excited state decays though the $6P_{3/2} \rightarrow 5S_{1/2}$ transition. Only 7.5% of the population excited into the $5D_{5/2}$ excited state generates 420-nm fluorescence through this pathway [33]. Decay from the excited state will return the atom to one of the two ground states as depicted in Fig. 1(a). By judicious excitation, through specific hyperfine states of the $5P_{3/2}$ or $5D_{5/2}$ energy levels, one finds that the selection rules ensure that the atom returns to its original hyperfine ground state. These *closed* transitions can be re-excited, creating a strong absorption and fluorescence. If the atom decays to the other unconnected ground state, following excitation through an *open* transition, then it will become dark as it can no longer interact with the light field.
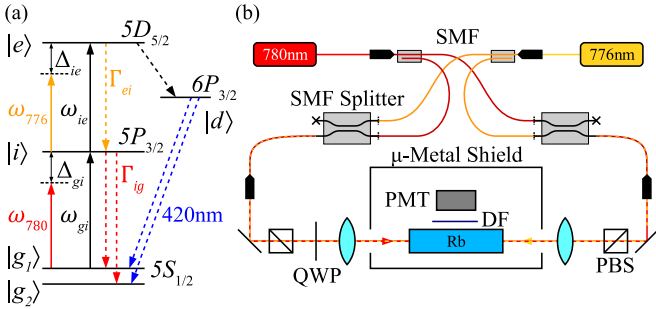
FIG. 1. (a) Energy level diagram of the two-photon transition. Solid arrows are driving lasers; dashed arrows show decay routes. (b) Schematic of the optical experimental setup. SMF, single mode fiber; PBS, polarizing beam splitter; QWP, quarter wave plate; DF, dichroic filter.

Figure 1(b) shows the optical setup and detection scheme. The 780-nm radiation was supplied by an extended cavity diode laser (ECDL), while the 776-nm radiation came from a titanium:sapphire laser (Ti:S). The linewidths of the ECDL and the Ti:S were measured to be 1.1 MHz and 50 kHz, respectively, over a 1-ms integration time measured against a stabilized frequency comb. Both lasers were coupled into single-mode optical fiber to ensure excellent spacial mode quality throughout the experiment and then could be coupled to the cell from either end or both simultaneously to produce copropagating or counterpropagating excitation lasers. To increase the two-photon transition rate, the lasers were focused using two 250-mm lenses to a $1/e^2$ radius spot-size of $\approx 62\,\mu$m within the center of the Rb cell. For the experiments shown here we used peak intensities of ≈ 80 and ≈ 400 kWm^{-2} for the 780- and 776-nm beams, respectively. The cell was surrounded with a μ-metal shield to minimize the magnetic field and was held at a temperature of $\approx 25\,°$C, corresponding to a vapor pressure of 1.3×10^{10} cm^{-3}. The 420-nm fluorescence was filtered using a narrowband blue light filter to prevent unwanted detection of scattered infrared light and then detected using a photomultiplier tube (PMT).

III. OBSERVED SPECTRA

We denote the two hyperfine $5S_{1/2}$ ground states $|g_1\rangle$ and $|g_2\rangle$, while the intermediate $5P_{3/2}$ and excited $5D_{5/2}$ states are denoted $|i\rangle$ and $|e\rangle$ with decay rates Γ_i and Γ_e, respectively, as illustrated in Fig. 1. In what follows, we refer to the $|g_{1,2}\rangle \rightarrow |i\rangle$ transition as the Rb D_2 transition.

Figure 2 shows two-dimensional maps displaying the dependence of the 420-nm fluorescence on the detuning of the 780-nm laser from the lower transition, $\Delta_{gi} = \omega_{gi} - \omega_{780}$, and the detuning of the 776-nm laser from the excited state, $\Delta_{ie} = \omega_{ie} - \omega_{776}$. These were obtained by scanning each laser over a 10-GHz interval centered on the single- and two-photon transitions. The maximum fluorescence is shown in black while while an absence of fluorescence is shown in white.

The two natural isotopes of Rb, ^{85}Rb and ^{87}Rb, have ground-state hyperfine splittings of ≈ 3.0 and ≈ 6.8 GHz, respectively, that give rise to four possible two-photon transitions. These are responsible for the strong diagonal features in Fig. 2, with
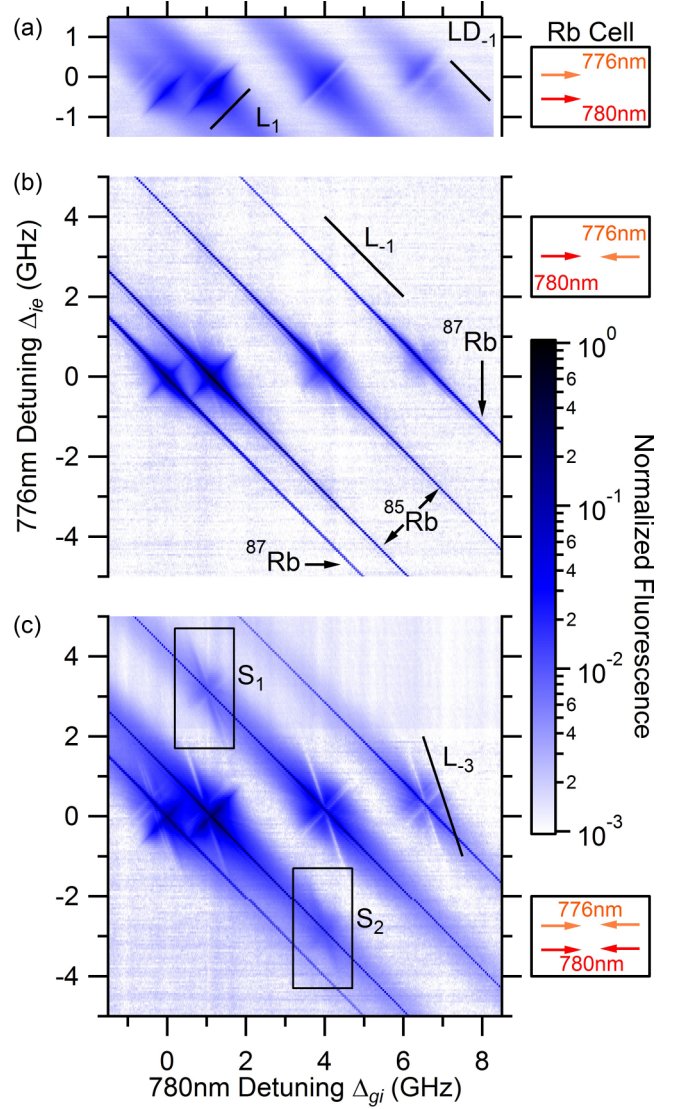

FIG. 2. Fluorescence spectra acquired with different incident laser configurations, shown to the right of the spectra. (a) Both lasers copropagating from a single direction producing Doppler-broadened lines, LD_{-1}, and Doppler-free lines, L_1. (b) Counterpropagating 780- and 776-nm lasers producing strong Doppler-free lines, L_{-1}. Small retroreflections from the Rb cell windows produce faint spectral components, LD_{-1} and L_1 lines. (c) Both lasers incident from both directions. In addition to the features described above, pronounced features with a gradient of -3, parallel to the line labeled L_{-3}, are observed. Increased fluorescent features above and below the main transitions of the ^{85}Rb isotope, indicated by boxes and labeled S_1 and S_2, are also observed, and also with a gradient of -3. The 780- and 776-nm detuning axes are centered on the $5S_{1/2}(F=3) \rightarrow 5P_{3/2}(F'=4)$ and $5P_{3/2}(F=4) \rightarrow 5D_{5/2}(F'=4)$ transitions respectively.

the two inner lines from excitation in ^{85}Rb and the outer two lines from ^{87}Rb.

We label the strong narrow features [full-width at half-maximum (FWHM) of ≈ 250 MHz along the Δ_{gi} axis] running with a $+1$ gradient in Figs. 2(a) and 2(c) as L_{+1}. We label the strong narrow features (FWHM of ≈ 20 MHz) running with a -1 gradient in Figs. 2(b) and 2(c) as L_{-1}. We also see features

with a gradient of -3 in Fig. 2(c), with a (FWHM of ≈ 20 MHz), which we labeled L_{-3} [which are also faintly evident in Fig. 2(b)]. We also see broader features (FWHM of ≈ 1 GHz) in Fig. 2(a) with a gradient of -1 that we labeled LD_{-1}. Below, we describe each of these features in greater detail.

A. $L_{\pm 1}$ and LD_{-1} lines

Figure 2(a) shows the resulting fluorescence observed when the 780- and 776-nm lasers are copropagating in the cell. We see that this gives rise to Doppler-broadened transitions, labeled LD_{-1}, as well as multiple bright fluorescence (dark blue) and reduced fluorescence (lighter blue) spectral features, labeled L_1, running with a $+1$ gradient.

In Fig. 2(b) we have arranged the 780- and 776-nm laser beams to be counterpropagating, which produces Doppler-free transitions, labeled L_{-1}. We also see some weak L_1 lines due to reflections from the flat cell windows producing some fluorescence features from the weak copropagating beams. We see that the L_{-1} and LD_{-1} features follow the empirical relationship

$$\Delta_{gi} + \Delta_{ie} = c, \tag{1}$$

while the L_1 features follow the empirical relationship

$$\Delta_{gi} - \Delta_{ie} = c, \tag{2}$$

where the offset c depends on the isotope and the hyperfine level. Equations (1) and (2) reflect conservation of energy, as two photons are absorbed through either Doppler-free two-photon excitation (counterpropagating) or Doppler-sensitive resonant two-step excitation (copropagating) configurations.

B. L_{-3} lines

Figure 2(c) shows the fluorescence from simultaneous co- and counterpropagating lasers. We see numerous features including Doppler-broadened, LD_{-1}, and Doppler-free fluorescence, L_{-1} and L_1, resulting from the processes outlined for Figs. 2(a) and 2(b). In addition, we see a set of additional bright fluorescence (dark blue) and reduced fluorescence (lighter blue) lines at a gradient of $-3.059(15)$, L_{-3} in Fig. 2(c). The width of these features indicates that they are close to Doppler free. The gradient of $-3.059(15)$ indicates an atom-light interaction in which the following empirical relationship is satisfied:

$$3\Delta_{gi} + \Delta_{ie} = c, \tag{3}$$

where the offset c depends on the isotope and the hyperfine level. We see an additional set of increased fluorescence features above and below the main transitions (labeled S_1 and S_2), which mimic the spectral features that are seen in Fig. 2(a).

We emphasize that the L_{-3} lines are only present when the 780-nm beam is incident on the cell from both directions while the 776-nm beam need only be incident from a single direction. No phase-matching was required to produce the L_{-3} features as might be expected if the process were a signature of four-wave mixing. Furthermore, no significant power dependence was observed upon the contrast of the L_{-3} lines when the power of each laser was varied by an order of magnitude. The L_{-3}, L_1, and L_{-1} features are seen to all intersect at the zero-velocity class atomic absorption to within 10 MHz. We also

compared this frequency to a second cell with a D_2 saturated absorption spectra, which confirms that this coincided with the zero-velocity class.

IV. MECHANISMS

The empirical relationships above give insight into the physical processes responsible for the spectral features. In part A of this section, we explain the $L_{\pm 1}$ and LD_{-1} features in terms of Doppler-free and Doppler-sensitive two-photon transitions. In part B, we describe three hypotheses that could produce the L_{-3} features and evaluate these hypotheses against numerical models.

A. Mechanism for $L_{\pm 1}$ and LD_{-1} lines

The resonances denoted by the labels L_{-1}, LD_{-1}, and L_1 in Fig. 2 are understood through transitions involving absorption of one 780-nm photon and one 776-nm photon to produce a transition to the excited state $|e\rangle$, which eventually decays back to the ground-state manifold.

A two-photon resonant transition occurs when the laser energies equal the energy difference between states $|g_1\rangle$ and $|e\rangle$, yielding

$$\Delta_{gi} + \Delta_{ie} = -v(k_{gi} \pm k_{ie}), \tag{4}$$

where k_{gi} and k_{ie} are the respective wave vectors of the 780- and 776-nm lasers, and v indicates the axial velocity class of atoms in two-photon resonance. The $\pm$ refers to excitation from copropagating $(+)$ or counterpropagating $(-)$ laser configurations. It can be seen that the left-hand side of Eq. (4) matches the left-hand side of Eq. (1), giving rise to the LD_{-1} and L_{-1} lines.

For copropagating laser fields, the right-hand side of Eq. (4) takes a Doppler-broadened range of values, $k_{gi} + k_{ie} \approx 2k_{ie}$, leading to the Doppler-broadened resonances, labeled LD_{-1} in Fig. 2(a). One expects to see a FWHM of 1.01 GHz, in excellent agreement with the observed value.

For counterpropagating laser fields, the wave-vectors on the RHS of Eq. (4) nearly cancel, $k_{gi} \approx k_{ie}$, giving only a very small dependence on axial atomic speed v. These lead to the Doppler-free resonances that have been labeled L_{-1} in Fig. 2(b).

Features with a gradient of 1 appear in Fig. 2(a), labeled L_1, as either enhanced fluorescence (dark blue) or reduced fluorescence (lighter blue) resonances in the copropagating configurations. These have a gradient of 1.019(2) and arise from a two-step excitation through the intermediate state. Simultaneous resonance with both transitions requires the laser detunings to be $\Delta_{gi} = -vk_{gi}$ and $\Delta_{ie} = -vk_{ie}$, respectively. Since $k_{ie}/k_{gi} = 1.005$, we find $\Delta_{gi} - \Delta_{ie} \approx 0$, corresponding to Eq. (2). This also explains Eq. (4) for copropagating beams.

Multiple transitions are observed for each of the ground-state hyperfine transitions arising from the intermediate-state hyperfine splitting [34] and efficient optical pumping on the $|g\rangle \rightarrow |i\rangle$ transition for atoms satisfying $\Delta_{gi} = -vk_{gi}$. Closed-cycle D_2 transitions, where population is continually recycled for reabsorption, produce bright fluorescence L_1 lines (dark blue), whereas open D_2 transitions, where population is pumped to the uncoupled ground state making it unavailable
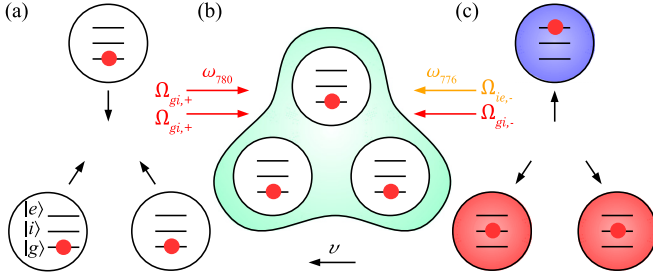
FIG. 3. Hypothesis 1: A proposed resonant process involving the collision of three atoms. Three atoms in their ground states collide (a) to form a metastable triatomic molecule (b). The molecule absorbs four photons, three from the ω_{780} field and one from the ω_{776} field, and decays into two singly excited atoms and one double-excited atom (c).

for reabsorption, produce reduced fluorescence L_1 lines (lighter blue). These transitions appear narrow due to velocity-selective optical pumping: the first resonant condition picks a particular velocity class, v, that can be excited, $\Delta_{gi} = -vk_{gi}$, while Eq. (4) means that there is a restriction on the detuning for the second excitation, $\Delta_{gi} = \Delta_{ie}$.

Equation (4) also predicts that the intersection of the L_{-1} and L_1 lines corresponds to the stationary velocity class of atoms. Verification of this was observed through comparison to a saturated absorption spectra of the $5S_{1/2} \to 5P_{3/2}$ transition.

B. Proposed mechanisms for L_{-3} lines

We propose three hypothetical mechanisms to explain the spectral features with a characteristic detuning gradient of ~ -3. These mechanisms are (i) collective triatomic absorption, in which a metastable triatomic molecular state resonantly absorbs four-photons simultaneously, (ii) excitation via amplified spontaneous emission, and (iii) optical population pumping between atomic ground states. These hypotheses all produce resonant features with a ~ -3 gradient, consistent with the observed L_{-3} lines.

For each mechanism, the atoms are modeled with two ground states, $|g_1\rangle$ and $|g_2\rangle$; an intermediate state, $|i\rangle$; an excited state, $|e\rangle$; and a state, $|d\rangle$, that facilitates additional decay paths as in Fig. 1(a). We use the excited-state population, P_e, as a proxy for the fluorescent intensity. In all cases, we consider J five-level atoms driven by applied laser fields.

The evolution of a collection of J optically driven atoms is governed by the optical Bloch master equations [35]:

$$\frac{d\rho}{dt} = -i[H,\rho] + \sum_{\substack{\text{atom } j=1}}^{J} \left(\Gamma_{e,i}^{(j)} \mathcal{D}[|i\rangle_j\langle e|]\rho + \Gamma_{e,d}^{(j)} \mathcal{D}[|d\rangle_j\langle e|]\rho \right.$$
$$+ \Gamma_{i,g_1}^{(j)} \mathcal{D}[|g_1\rangle_j\langle i|]\rho + \Gamma_{i,g_2}^{(j)} \mathcal{D}[|g_2\rangle_j\langle i|]\rho$$
$$\left. + \Gamma_{d,g_1}^{(j)} \mathcal{D}[|g_1\rangle_j\langle d|]\rho + \Gamma_{d,g_2}^{(j)} \mathcal{D}[|g_2\rangle_j\langle d|]\rho \right), \quad (5)$$

where $\mathcal{D}$ indicates a Lindblad superoperator [35] generating relaxation at the rate Γ. The Hamiltonian for the system of atoms is $H = \sum_j H_j + H_{dd}$, where, for $J > 1$, H_{dd} is an interatomic dipole-dipole coupling Hamiltonian. H_j is the
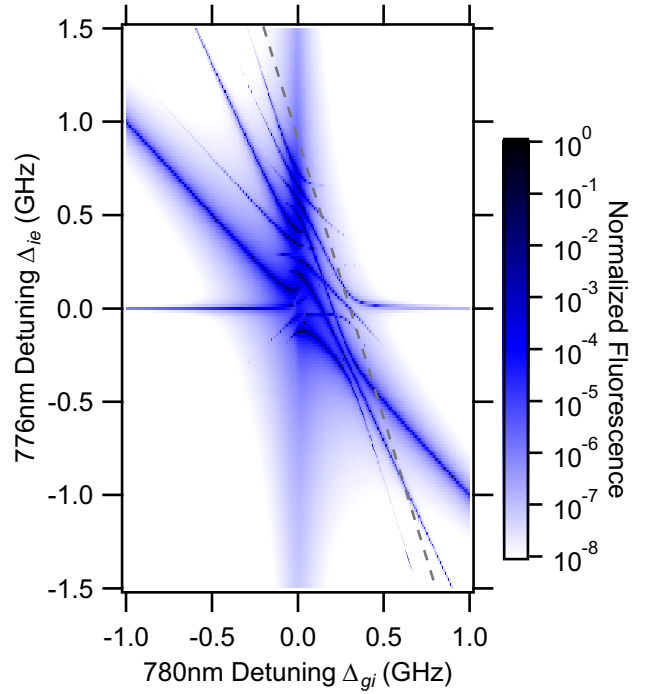

FIG. 4. Model 1: Excited state populations, P_e, for the triatomic collision model. Here we take $\Omega_{ie,-} = \Omega_{gi,+}/100$, $\Omega_{gi} \gg \Gamma_{ab}$, and $v_{ie}/r_{jk}^3 = 8$ as arbitrary but illustrative quantities. We have shown only the stationary, $v = 0$, velocity class. The dashed line has a gradient of -3.

Hamiltonian for atom j:

$$H_j = \epsilon_e |e\rangle_j\langle e| + \epsilon_i |i\rangle_j\langle i| + \Omega_{ie}(t)X_{ie}^{(j)} + \Omega_{g_1i}(t)X_{g_1i}^{(j)},$$

where $X_{ab}^{(j)} = |a\rangle_j\langle b| + |b\rangle_j\langle a|$ and ϵ_a is the energy of level $|a\rangle$. The external laser driving is given by

$$\Omega_{ab}(t) = \Omega_{ab,+}\cos\left[(\omega_{ab} + \Delta_{ab} + k_{ab}v)t\right]$$
$$+ \Omega_{ab,-}\cos\left[(\omega_{ab} + \Delta_{ab} - k_{ab}v)t\right],$$

where v is the axial component of the atomic velocity, ω_{ab} is the $|a\rangle \leftrightarrow |b\rangle$ transition frequency, Δ_{ab} is the optical detuning from this transition, and $\Omega_{ab,\pm} = d_{ab}E_{ab,\pm}$ are the corresponding Rabi frequencies for the field propagating in the directions that are Doppler upshifted $(+)$ or downshifted $(-)$. The dynamics of this system depend on the detunings $\Delta_{gi} = \omega_{gi} - \omega_{780}$ and $\Delta_{ie} = \omega_{ie} - \omega_{776}$.

L_{-3} Hypothesis 1: Triatomic four-photon absorption. In this hypothesis, we consider a $J = 3$ atom model which describes a metastable triatomic molecular bound state moving with some velocity v, as shown in Fig. 3(b). This molecular state can absorb four photons, three at ω_{780} and one at ω_{776}, and then dissociate to three unbound atoms, two in a singly-excited state and the third in a doubly excited state. This process is resonant when

$$(\omega_e - \omega_g) + 2(\omega_i - \omega_g) = 3\omega_{780} + \omega_{776}$$
$$= 3(\omega_{gi} - \Delta_{gi}) + (\omega_{ie} - \Delta_{ie}). \quad (6)$$

Since $(\omega_e - \omega_g) + 2(\omega_i - \omega_g) = 3\omega_{gi} + \omega_{ie}$, this implies Eq. (3). We note that for the combination of laser directions
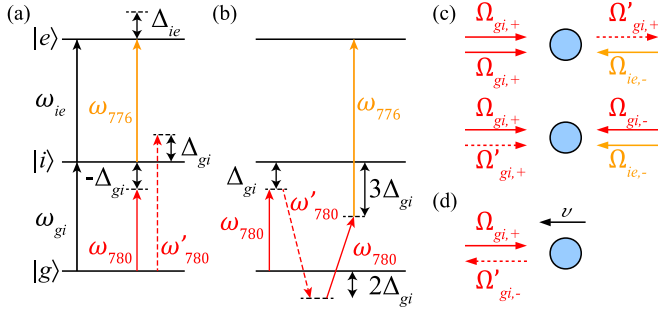
FIG. 5. Hypothesis 2: A proposed resonant, Doppler-free, four-photon process. (a) Atoms are illuminated with light at frequencies ω_{780} and ω_{776}. We further hypothesize the existence of another field at ω'_{780}, but with the opposite detuning to the imposed field ω_{780}; a mechanism for the autonomous, resonant production of this field is described in the text. (b) Resonant four-photon transition in which two ω_{780} photons and one ω_{776} photon are absorbed, accompanied by stimulated emission of a photon into the ω'_{780} field. (c) Configurations of four beams that produce Doppler-free transitions. (d) Seeding the ancillary field ω'_{780} by backscattering the applied field ω_{780} from a Doppler-resonant atom; the stimulated process in panel (b) will then self-consistently amplify the seed field.
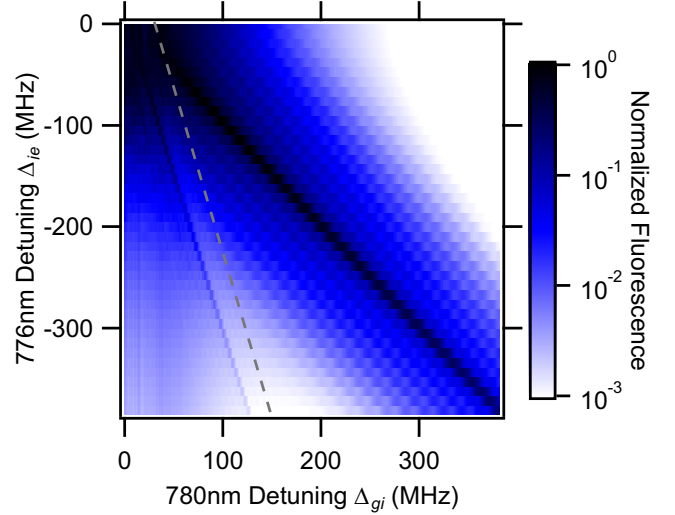

FIG. 6. Model 2: Excited-state population, P_e, for the amplified spontaneous emission process. Here we take $\Omega_{gi,\pm} = \Omega'_{gi,\pm} = \Omega_{ie,-} = 100\Gamma_{gi}$ and $\Gamma_{ie} = \Gamma_{gi}$ as arbitrary but illustrative quantities. LD_{-1}, $L_{\pm1}$, and L_{-3} lines are all generated. The dashed line has a gradient of -3.

shown in Fig. 3(b), this process is Doppler free; i.e., Doppler shifts of the different fields cancel.

Interactions between atoms, mediated via long-range dipole-dipole coupling, have been observed in dense ultracold atomic clouds, with densities of $\approx 10^{11}$ cm^{-3}, to alter the absorptive properties of atomic vapors [27–29].

Two-atom resonances have recently been reported in a hot (≈ 400 K) potassium vapor and in rubidium [24] arising from coherent dipole-dipole coupling between atoms. Triatomic bound states have received attention in observations of Efimov states, which exhibit a universal ladder of bound-state energies [36,37]. Numerical simulations of chaotic dynamics in a classical triatomic system exhibit metastable triatomic states [31]. At low energies, these simulations show long metastable triatomic lifetimes of 10 to 100 ns; however this falls to ~10 ps at 300 K, where our experiments are performed.

To model this hypothesis, we include an interatomic dipole-dipole coupling Hamiltonian that captures the weak collisional shifts depicted in Fig. 3:

$$H_{dd} = v_{ie} \sum_{j,k=1}^{J=3} X_{ie}^{(j)} X_{ie}^{(k)} / r_{jk}^3. \tag{7}$$

The dipole-dipole coupling strength is v_{ie}, and r_{jk} is the interatomic distance. A closed atomic model was used that did not include the uncoupled state, $|g_2\rangle$, or additional decay paths, $|d\rangle$, i.e., $\Gamma_{e,d}^{(j)} = \Gamma_{d,g_{1,2}}^{(j)} = \Gamma_{i,g_2}^{(j)} = 0$.

The symmetric state $\overline{|iie\rangle} = (|iie\rangle + |iei\rangle + |eii\rangle)/\sqrt{3}$ has energy $\overline{\langle iie|H|iie\rangle} \approx 3\Delta_{gi} + \Delta_{ie} - 2v_{ie}/r^3$, so we expect a resonance when laser photon energies sum to this. This condition has the same gradient as Eq. (3), with a constant offset given by the binding energy $2v_{ie}/r^3$.

Figure 4 shows the steady-state excited-state probability P_e versus detunings for this model (for a stationary velocity class). There are lines corresponding to the various processes

allowed in this interaction, including L_{-1}. There is a (faint) resonance corresponding to L_{-3} (running parallel to and below the indicative dashed gray line), which follows the resonance condition $3\Delta_{gi} + \Delta_{ie} = 2v_{ie}/r^3$.

Binding energies in triatomic bound states are $\lesssim 1$ cm^{-1} corresponding to a frequency of ~3 GHz [27], and so we would expect this mechanism to produce shifts for the L_{-3} line of this order in Fig. 2. This is not consistent with the experimental observations, in which the features L_{-3}, L_1, and L_{-1} all cross within 10 MHz of the zero-velocity class of atoms.

L_{-3} Hypothesis 2: Amplified spontaneous emission. Figure 5 shows a process in which a single atom undergoes a four-photon transition to the double-excited state. In this scenario, as well as for the imposed fields at ω_{780} and ω_{776}, we hypothesis the existence of an auxiliary, spontaneously generated field at $\omega'_{780} \approx \omega_{780}$. This auxiliary field is proposed to have a frequency that depends on ω_{780} but with an equal but opposite detuning from ω_{gi}, i.e., $\omega_{780} = \omega_{gi} - \Delta_{gi}$ and $\omega'_{780} = \omega_{gi} + \Delta_{gi}$. Below we suggest a self-consistent mechanism to generate the auxiliary field, but first we assume its presence.

If these three fields are coincident on an atom, there is a four-photon resonant process consisting of absorption of two photons at frequency ω_{780} and one at ω_{776}, along with the stimulated emission of a fourth photon at ω'_{780}, as depicted in Fig. 5(b). This process is resonant when

$$\begin{aligned} \omega_e - \omega_g &= 2\omega_{780} - \omega'_{780} + \omega_{776} \\ &= 2(\omega_{gi} - \Delta_{gi}) - (\omega_{gi} + \Delta_{gi}) + (\omega_{ie} - \Delta_{ie}), \end{aligned} \tag{8}$$

which implies Eq. (3) since $\omega_e - \omega_g = \omega_{gi} + \omega_{ie}$. We note that for the combination of laser directions shown in Fig. 5(c), this process is Doppler free; i.e., Doppler shifts of the different fields cancel. In this process, the auxiliary field is self-consistently amplified: the resonant process drives further production of light at frequency ω'_{780}.
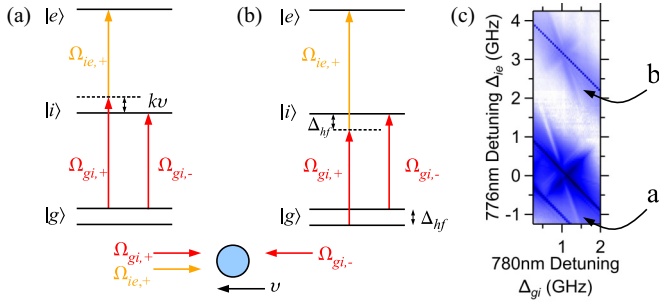
FIG. 7. Hypothesis 3: Optical pumping for (a) the strong stepwise transition and (b) the shadow observed in the other ground state both highlighted in the data (c). Detunings from the intermediate state are shown (not to scale) where kv is a detuning of a Doppler shift and Δ_{hf} is ground-state splitting of Rb being ≈ 3 and ≈ 6 GHz for the ^{85}Rb and ^{87}Rb isotopes, respectively.

It remains to identify a process capable of seeding the auxiliary field ω'_{780}, whose detuning is locked to that of ω_{780} (albeit with opposite sign). Consider an atomic velocity class that is resonant with the driving field ω_{780}, so that in the atomic frame $\omega_{780} = \omega_{gi}$. These atoms will be resonantly excited to the intermediate state, from which they decay by spontaneous emission. This spontaneously emitted light is emitted in all directions; however for the component emitted in the direction antiparallel to the absorbed light (i.e., backscattered), we see that it will be Doppler shifted to the required frequency, ω'_{780}, as depicted in Fig. 5(d). Thus, light that is resonantly backscattered from a suitable atomic velocity class will be at the correct frequency to seed the self-amplifying process described above.

To model this hypothesis, where $J = 1$ and $H_{dd} = 0$, the atomic Hamiltonian under the rotating-wave approximation is

$$
\begin{aligned}
H = {}& \Delta_{gi}|i\rangle\langle i| + (\Delta_{gi} + \Delta_{ie})|e\rangle\langle e| \\
& + \tfrac{1}{2}[(\Omega_{gi,+}e^{itvk} + \Omega_{gi,-}e^{-itvk})|i\rangle\langle g_1| \\
& + (\Omega'_{gi,+}e^{it(\Delta_{gi}+vk)} + \Omega'_{gi,-}e^{it(\Delta_{gi}-vk)})|i\rangle\langle g_1| \\
& + (\Omega_{ie,+}e^{itvk} + \Omega_{ie,-}e^{-itvk})|e\rangle\langle i| + \text{H.c.}]. \quad (9)
\end{aligned}
$$

A closed atomic model was used that did not include the uncoupled state, $|g_2\rangle$, or additional decay paths, $|d\rangle$, i.e., $\Gamma_{e,d}^{(j)} = \Gamma_{d,g_{1,2}}^{(j)} = \Gamma_{i,g_2}^{(j)} = 0$.

Figure 6 shows the steady-state excited-state probability P_e, averaged over a Gaussian distribution of velocities, assuming the applied fields and the induced field all have the same strength, $\Omega_{gi,\pm} = \Omega'_{gi,\pm} = \Omega_{ie,-}$. Along the main diagonal is the expected Doppler-free two-photon resonance, L_{-1}, with a broad "halo", LD_{-1}, arising from doubly resonant transitions for atoms in different velocity classes. Also evident is a feature consistent with the L_{-3} line (parallel to and below the dashed line).

We note that this model does not account for the hypothesized generation and amplification of the ancillary field, ω'_{gi}, depicted in Fig. 5; rather, it is included phenomenologically. A more sophisticated three-dimensional model could couple the ancillary field amplitude to the population dynamics required to amplify this field; however we do not consider this here.
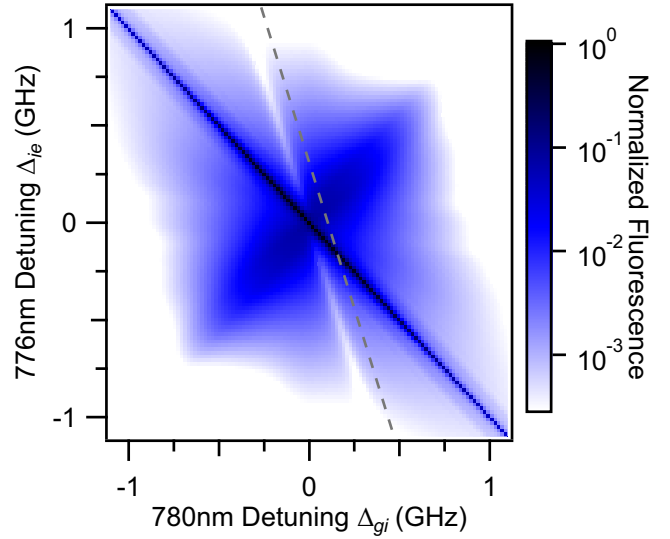

FIG. 8. Model 3: Excited-state population, P_e, for the population pumping model. Model parameters were $\Omega_{gi,\pm} = \Gamma_i$ and $\Omega_{ie,+} = \Gamma_i/10$. LD_{-1}, $L_{\pm 1}$, and L_{-3} lines are all generated. The dashed line has a gradient of -3.

L_{-3} Hypothesis 3: Population pumping. Population pumping forms the basis of the third hypothetical process for creating the L_{-3} lines, as depicted in Fig. 7(a). In this hypothesis, there is a competition between the two-photon resonant excitation to the excited state and the single-photon resonance $|g_1\rangle \rightarrow |e\rangle$.

In particular, consider the situation in which a particular velocity class, v, is two-photon resonant for copropagating fields $\omega_{780,+}$ and $\omega_{776,+}$. In the laboratory frame, we have $\Delta_{g_1 i} + \Delta_{ie} = 2kv$.

It may also happen that velocity class v is single-photon resonant ($|g_1\rangle \rightarrow |i\rangle$) for the counterpropagating field $\omega_{780,-}$. This occurs if $\Delta_{g_1 i} = -kv$. In this situation, the single-photon transition drives population into $|i\rangle$, which can then relax to an uncoupled ground state $|g_2\rangle$ [see Fig. 7(a)], so that the atom becomes dark.

These two conditions (two-photon resonance for copropagating beams and one-photon resonance for counterpropagating $\omega_{780,-}$) both occur simultaneously when $3\Delta_{g_1 i} + \Delta_{ie} = 0$. That is, along the L_{-3} line, the single-photon process pumps atoms to a dark state, suppressing Doppler-resonant two-photon driven fluorescence.

The same mechanism also generates shadow L_{-3} features, $S_{1,2}$ shown in Fig. 2(c), through the mechanism depicted in Fig. 7(b). In this case, there is a two-photon resonance between $|g_2\rangle$ and $|e\rangle$ for copropagating fields, but a one-photon resonance between $|g_1\rangle$ and $|i\rangle$ for the counterpropagating field at ω_{780}.

In the interaction picture, where $J = 1$ and $H_{dd} = 0$, the Hamiltonian under the rotating-wave approximation for the population pumping mechanism is given by

$$
\begin{aligned}
H = {}& \Delta_{gi}|i\rangle\langle i| + (\Delta_{gi} + \Delta_{ie})|e\rangle\langle e| + \omega_d|d\rangle\langle d| \\
& + \tfrac{1}{2}[(\Omega_{gi,+}e^{itvk} + \Omega_{gi,-}e^{-itvk})|i\rangle\langle g_1| \\
& + (\Omega_{ie,+}e^{itvk})|e\rangle\langle i| + \text{H.c.}]. \quad (10)
\end{aligned}
$$

This model included all the atomic states shown in Fig. 1 incorporated with known branching ratios [33,34,38–40].

Figure 8 shows numerical simulations of $P_e(\Delta_{ie}, \Delta_{gi})$ averaged over a Gaussian distribution of velocities and integrated over an average beam crossing time, when $\Omega_{gi,\pm} = \Gamma_i$ and $\Omega_{ie,+} = \Gamma_i/10$. The Doppler-free, $L_{\pm 1}$, and the Doppler broadened, LD_{-1}, lines are evident. A clear spectral feature consistent with an L_{-3} line is also visible (running parallel and below the indicative dashed gray line).

V. DISCUSSION

Here we compare the proposed hypotheses against experimental observations. We reiterate that not all of our models include the full state description of the atoms and hence have not included transitions out of the $|i\rangle$ or $|e\rangle$ states into dark ground states $|g_2\rangle$, which would deplete the population of optically active atoms in the $|g_1\rangle$ state and result in reduced fluorescence. Instead, these models merely establish resonance conditions in which the excited state has significant population, which may lead to a subsequent cascade if available. All the hypotheses exhibit resonances with a gradient matching the L_{-3} feature. However each have additional characteristics that discriminate amongst them and the experimental observations.

First, we consider the triatomic hypothesis. Under the ambient conditions of the experiment, the lifetime of these states is predicted to be very short [31], and so the available density of molecules is likely to be insignificant. Furthermore, the binding energy of the state, typically tens of GHz [27], would be observed in the two-photon spectroscopic data as an offset in the crossing of the feature L_{-3} with respect to $L_{\pm 1}$. As the experimental data do not show any such offset, we rule out the triatomic collision hypothesis.

Second, we consider the hypothesis in which atomic excitation proceeds with the assistance of an auxiliary field produced by amplified stimulated emission. Figure 6 shows an L_{-3} resonance which bears some resemblance to the experimental data in Fig. 2(c). One testable prediction of this hypothesis is the existence of the auxiliary field ω'_{780}. If it were present, this field could be detected by observing an interference between the applied ω_{780} field and the new auxiliary field; since these fields have equal but opposite detunings from ω_{gi}, one would expect a mixing product at $2\Delta_{gi}$. Furthermore, one expects a good spatial overlap between these two beams as our

proposed generation mechanism ensures that it will track the applied beam. We have made attempts to detect this mixing frequency but it was not observed, leading us to believe that the amplified spontaneous emission hypothesis is probably not the explanation for the features.

The third hypothesis, involving optical pumping, yields a two-photon absorption spectrum, Fig. 8, that qualitatively matches the experimentally observed data shown in Fig. 2(c). We clearly see that the model predicts a reduced fluorescence L_{-3} line, along with the clearly visible $L_{\pm 1}$ and LD_{-1} lines which match experimental observations. Furthermore, this hypothesis also explains the shadow fluorescence features, $S_{1,2}$, in Fig. 2 that arise from population pumping through the various hyperfine states in the intermediate state, illustrated in Fig. 7(b).

VI. CONCLUSION

We have observed surprising spectral features in the fluorescence of a two-photon transition in a room-temperature rubidium vapor as we adjust the driving frequencies of the two lasers. We have considered three hypothetical mechanisms to explain these spectral features, each of which is broadly consistent with the energetics of the observed behavior. The first hypothetical mechanism was a triatomic resonance, but this was ruled out, due to both the numerically predicted low density (short lifetime) of such states and the absence of any signature of the binding energy of such a resonance. The second hypothetical mechanism was an amplified spontaneous emission process to generate an auxiliary field, enabling a resonant four-photon transition. Experimental evidence for this auxiliary field was not seen, ruling out this hypothesis as an explanation for the observations. The final hypothetical mechanism involved optical population pumping out of the atomic ground state to produce a resonance that has characteristics that are consistent with the observed data, leaving optical pumping as the most promising explanation.

---

*Deceased as of May 21, 2016.

[1] M. Fleischhauer, A. Imamoglu, and J. Marangos, Rev. Mod. Phys. **77**, 633 (2005).

[2] K.-J. Boller, A. Imamoglu, and S. E. Harris, Phys. Rev. Lett. **66**, 2593 (1991).

[3] A. M. Akulshin, S. Barreiro, and A. Lezama, Phys. Rev. A **57**, 2996 (1998).

[4] A. Lezama, S. Barreiro, and A. M. Akulshin, Phys. Rev. A **59**, 4732 (1999).

[5] H. R. Gray, R. M. Whitley, and C. R. Stroud, Opt. Lett. **3**, 218 (1978).

[6] A. S. Zibrov, M. D. Lukin, D. E. Nikonov, L. Hollberg, M. O. Scully, V. L. Velichansky, and H. G. Robinson, Phys. Rev. Lett. **75**, 1499 (1995).

[7] C. Andreeva, G. Bevilacqua, V. Biancalana, S. Cartaleva, Y. Dancheva, T. Karaulanov, C. Marinelli, E. Mariotti, and L. Moi, Appl. Phys. B **76**, 667 (2003).

[8] S. Pradhan, A. Kani, H. Wanare, R. Behera, and A. K. Das, Phys. Rev. A **85**, 063805 (2012).

[9] H. Schmidt and A. Imamoglu, Opt. Lett. **21**, 1936 (1996).

[10] H.-Y. Lo, Y.-C. Chen, P.-C. Su, H.-C. Chen, J.-X. Chen, Y.-C. Chen, I. A. Yu, and Y.-F. Chen, Phys. Rev. A **83**, 041804 (2011).

[11] M. Bajcsy, S. Hofferberth, V. Balic, T. Peyronel, M. Hafezi, A. S. Zibrov, V. Vuletic, and M. D. Lukin, Phys. Rev. Lett. **102**, 203902 (2009).

[12] A. M. Akulshin, R. J. McLean, A. I. Sidorov, and P. Hannaford, Opt. Express **17**, 22861 (2009).

[13] A. M. Akulshin, A. A. Orel, and R. J. McLean, J. Phys. B **45**, 015401 (2012).

[14] J. Vanier, Appl. Phys. B **81**, 421 (2005).

[15] S. Knappe, V. Shah, P. D. D. Schwindt, L. Hollberg, J. Kitching, L.-A. Liew, and J. Moreland, Appl. Phys. Lett. **85**, 1460 (2004).

[16] J. Bjorkholm and P. Liao, Phys. Rev. A **14**, 751 (1976).

[17] B. C. Jacobs and J. D. Franson, Phys. Rev. A **79**, 063830 (2009).

[18] D. A. Braje, V. Balić, G. Y. Yin, and S. E. Harris, Phys. Rev. A **68**, 041801 (2003).

[19] B. C. Jacobs, T. B. Pittman, and J. D. Franson, Phys. Rev. A **74**, 010303 (2006).

[20] J. D. Franson, B. C. Jacobs, and T. B. Pittman, Phys. Rev. A **70**, 062302 (2004).

[21] S. M. Hendrickson, M. M. Lai, T. B. Pittman, and J. D. Franson, Phys. Rev. Lett. **105**, 173602 (2010).

[22] L. Hilico, R. Felder, D. Touahri, O. Acef, A. Clairon, and F. Biraben, Eur. Phys. J. Appl. Phys. **4**, 219 (1998).

[23] M. Poulin, C. Latrasse, D. Touahri, and M. Têtu, Opt. Commun. **207**, 233 (2002).

[24] X. Dai, M. Richter, H. Li, A. D. Bristow, C. Falvo, S. Mukamel, and S. T. Cundiff, Phys. Rev. Lett. **108**, 193201 (2012).

[25] Y.-Q. Zhang, L. Tan, and P. Barker, Phys. Rev. A **89**, 043838 (2014).

[26] L. Bruder, M. Binz, and F. Stienkemeier, Phys. Rev. A **92**, 053412 (2015).

[27] J. Pérez-Ríos, M. Lepers, and O. Dulieu, Phys. Rev. Lett. **115**, 073201 (2015).

[28] S. M. Farooqi, D. Tong, S. Krishnan, J. Stanojevic, Y. P. Zhang, J. R. Ensher, A. S. Estrin, C. Boisseau, R. Côté, E. E. Eyler, and P. L. Gould, Phys. Rev. Lett. **91**, 183002 (2003).

[29] D. Tong, S. M. Farooqi, J. Stanojevic, S. Krishnan, Y. P. Zhang, R. Côté, E. E. Eyler, and P. L. Gould, Phys. Rev. Lett. **93**, 063001 (2004).

[30] M. D. Lukin, M. Fleischhauer, R. Cote, L. M. Duan, D. Jaksch, J. I. Cirac, and P. Zoller, Phys. Rev. Lett. **87**, 037901 (2001).

[31] J. F. E. Croft and J. L. Bohn, Phys. Rev. A **89**, 012714 (2014).

[32] F. Nez, F. Biraben, R. Felder, and Y. Millerioux, Opt. Commun. **102**, 432 (1993).

[33] D. Sheng, A. Pérez Galván, and L. A. Orozco, Phys. Rev. A **78**, 062506 (2008).

[34] D. A. Steck, Rubidium 87 D line data, http://steck.us/alkalidata (Revision 2.1.5, 13 January 2015).

[35] D. F. Walls and G. J. Milburn, *Quantum Optics* (Springer-Verlag, Berlin, 2008).

[36] E. Braaten and H.-W. Hammer, Phys. Rep. **428**, 259 (2006).

[37] E. Braaten and H.-W. Hammer, Ann. Phys. **322**, 120 (2007).

[38] M. S. Safronova, C. J. Williams, and C. W. Clark, Phys. Rev. A **69**, 022509 (2004).

[39] J. E. Sansonetti, J. Phys. Chem. Ref. Data **35**, 301 (2006).

[40] M. S. Safronova and U. I. Safronova, Phys. Rev. A **83**, 052508 (2011).